Met. Mater. Int., Vol. 18, No. 2 (2012), pp. 217~223
doi: 10.1007/s12540-012-2003-9 Published 27 April 2012

Effect of Tungsten Addition on the Mechanical Properties and Corrosion Resistance of S355NL Forging Steel

Jingwei Zhao[1], Yong Woo Kim[1], Jeong Hun Lee[1], Jin Mo Lee[2], Hi Sang Chang[2], and Chong Soo Lee[1,*]

[1]Department of Materials Science and Engineering, and Graduate Institute of Ferrous Technology, Pohang University of Science and Technology, Pohang 790-784, Korea
[2]Taewoong Co. Ltd., 1462-1, SongJeong-Dong, Gangseo-Gu, Busan 618-270, Korea

(received date: 11 April 2011 / accepted date: 2 September 2011)

A study was made to investigate the effect of tungsten (W) addition on the microstructure, tensile properties, Vickers hardness, and corrosion resistance of S355NL forging steel. Mechanical properties were evaluated and considered in the context of the interlamellar spacing of pearlite. Microstructural analysis revealed that the addition of W favors the formation of intragranular acicular ferrite and leads to a decrease in the interlamellar spacing of pearlite. After W addition, the corrosion rust film was intact. The steel containing W showed fewer microcracks distributed in the corroded surface compared with that without W. It was concluded that the addition of W is beneficial for improvement of both the mechanical properties and corrosion resistance of S355NL forging steel.

Key words: metals, forging, mechanical properties, corrosion, tungsten

1. INTRODUCTION

High-strength forging steels are typically manufactured by quenching and tempering followed by hot forging. This multi-stage process extends production time and leads to higher production costs. Instead, microalloyed steels, which achieve their strength during air cooling after forging, have been developed to realize cost savings. The air-cooled microstructure of microalloyed forging steels is generally composed of coarse ferrite and pearlite. Since the strength improvement of the microalloyed ferritic-pearlitic steels mainly depends on the increment of pearlite volume fraction, ferrite grain refinement, solid solution, and precipitation strengthening, it is limited to obtain a higher level of strength, leading to an obstacle to the development of its potential uses. It therefore becomes an important issue to increase the strength of ferritic-pearlitic steels, and several attempts have been made to achieve this goal through alloy modification [1-4].

Steels used for marine structures require not only excellent strength to bear heavy loads, but also high performance in corrosion resistance under the conditions of exposure to sunshine, rain, and sea water. As a base metal commonly used in marine structures, S355NL steel, a high-strength low-alloy (HSLA) steel consisting of ferrite and pearlite, has been widely investigated to meet these requirements. Several studies based on existing S355NL steel have paid more attention to abrasion resistance and fatigue behaviors [5-8]. However, research on improving both the strength and corrosion resistance of S355NL by alloying has rarely been conducted. Since the use of S355NL-base steels is expected to increase, especially in marine structures, it is important to develop S355NL-base steels possessing higher strength and excellent corrosion resistance.

Because tungsten (W) can restrain pearlite and ferrite transformations, W is widely used as a grain refiner and solid solution reinforcement to improve the mechanical properties of steels [9-12]. In addition, corrosion resistance can be enhanced by alloying of W in steels [13-16]. However, systematic work concerning the effect of W on the mechanical properties and corrosion resistance of S355NL steel has not been reported so far. This study, therefore, focused on the effect of W addition on the microstructure, mechanical properties, and corrosion resistance of S355NL forging steel with investigation of the influence mechanism of W on microstructural evolution and mechanical properties.

2. EXPERIMENTAL PROCEDURE

The materials used in this study were three kinds of S355NL steels with different contents of W. The chemical compositions are shown in Table 1. Ingots of the three alloys

*Corresponding author: cslee@postech.ac.kr

Table 1. Chemical compositions (wt%) of the steels investigated

Specimens	C	Mn	Cr	Ni	Cu	Si	Al	V	Nb	Ti	P	S	N	W
C1	0.17	1.2	0.1	0.02	0.02	0.47	0.02	0.01	0.02	0.02	0.01	0.01	0.006	–
CW1	0.17	1.2	0.1	0.02	0.02	0.47	0.02	0.01	0.02	0.02	0.01	0.01	0.006	0.1
CW5	0.17	1.2	0.1	0.02	0.02	0.47	0.02	0.01	0.02	0.02	0.01	0.01	0.006	0.5

were fabricated by vacuum induction melting and then hot forged, followed by air cooling. Cylindrical forged ingots with a diameter of 100 mm and a height of 600 mm were obtained. Central parts near the axis of the forged ingots were taken as the study object.

To evaluate the mechanical properties, tensile tests were performed using standard specimens (Gauge length 25 mm, gauge diameter 6 mm) on an Instron 8801 tensile testing machine at room temperature with a strain rate of 5×10^{-3} s^{-1}. The yield strength (YS, 0.2 % proof stress), ultimate tensile strength (UTS), and percentage of elongation were recorded directly from the results displayed by computer on a monitor. Hardness was measured with a Vickers hardness tester using a 2 kg load and a 10 s dwelling time, and indentations were made randomly on the specimen surfaces.

To analyze the effect of W addition on the corrosion resistance of the experimental steels, potentiostatic/galvanostatic measurement was employed. To measure the corrosion potential of the steels, potentiodynamic anodic polarization tests were conducted in 3.5 wt% NaCl solution at room temperature. To study the effect of the NaCl solution concentration on corrosion resistance, a milder solution with 1 wt% NaCl was also employed in the corrosion tests. One side of the specimen was mechanically polished with 2400 grit SiC sandpaper. The corrosion area of the specimen was defined as 1 cm^2. The tests were conducted at a potential range of 0 to +300 mV_{SCE} and a scanning rate of 0.5 mV s^{-1}.

The specimens were metallographically polished and etched with 2 % nital solution for microstructural observation by optical microscope (OM). Slightly overetched specimens were examined under a scanning electron microscope (SEM). The volume fractions of intragranular acicular ferrite (IAF) and pearlite were measured on 10 randomly selected fields at a magnification of ×100 in the OM. Fifty random SEM images at magnifications from ×5000 to ×7000 without bias were made to measure the interlamellar spacing of pearlite. Transmission electron microscopy (TEM) was employed to investigate the high-resolution structure. All the TEM specimens were prepared by using a focused ion beam (FIB) method. The fracture and corrosion surfaces of the tested specimens were observed by SEM.

3. RESULTS AND DISCUSSION

3.1. Microstructure

3.1.1. Effect of W on the microstructure

Figure 1 shows the typical microstructures of the C1, CW1, and CW5 forging steels. As shown in Figs. 1(a) and (d), C1 steel consists mainly of polygonal ferrite (PF) and pearlite, besides a small quantity of IAF (the volume fraction

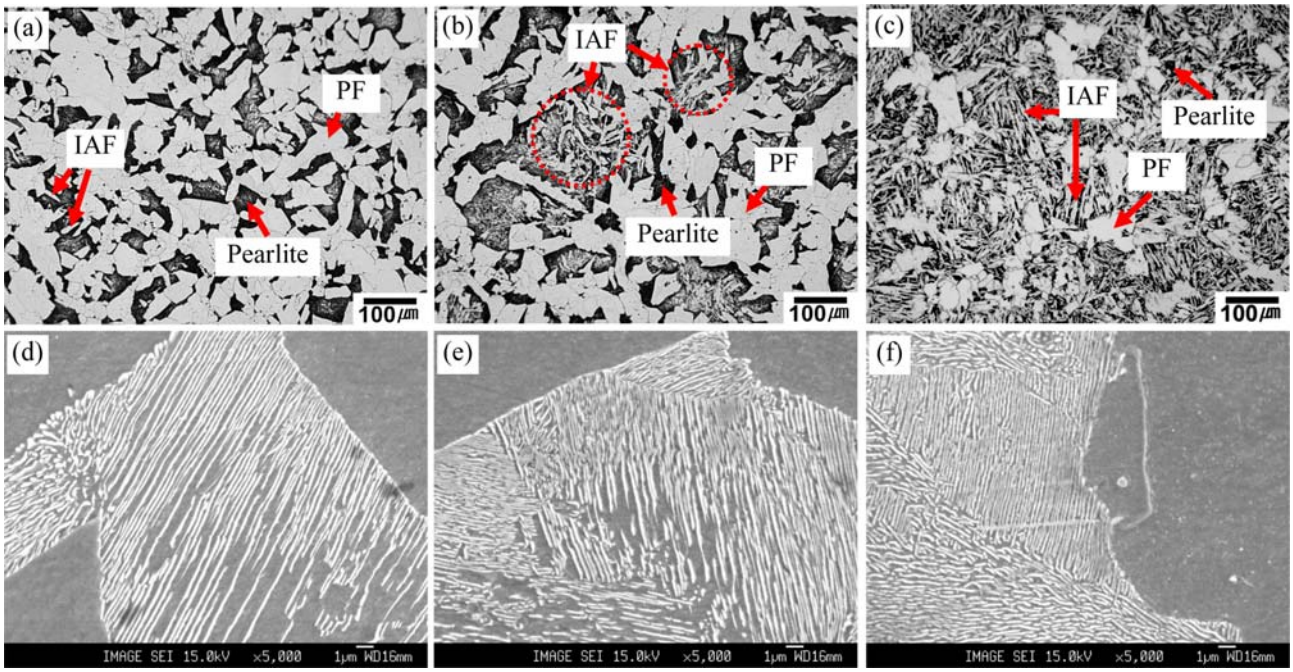

Fig. 1. Microstructures of C1 (a,d), CW1 (b,e), and CW5 (c,f) steels. (a,b,c) OM structures; (d,e,f) SEM of pearlite.

was measured to be 5 %). The addition of W leads to a change in the microstructure (Figs. 1(b), (c), (e) and (f)). The volume fractions of IAF were measured to be 22 % and 51 % in CW1 and CW5 steels, respectively. The amount of IAF greatly increased after W addition, and the higher the content of W that is added, the higher the amount of IAF that can be obtained.

To understand the formation of IAF in forging steel, the nucleation mechanism of IAF was analyzed. It is widely accepted that the nucleation of IAF takes place inside austenite grains on nonmetallic inclusions [17-20]. Nonmetallic inclusions can be oxides or other compounds, but the important point is that they may stimulate acicular ferrite [21]. The nucleation of a single plate on an inclusion can in turn stimulate others to nucleate autocatalytically, so that a one-to-one correspondence between the number of active inclusions and the number of acicular ferrite plates is not expected [22]. Plates of IAF nucleate heterogeneously on small nonmetallic inclusions and radiate in many different directions from these point nucleation sites. IAF does not grow in sheaves because their development is stifled by impingement between plates nucleated independently at adjacent sites [23]. A schematic diagram of IAF formation is shown in Fig. 2.

Microalloyed forging steels are usually deformed at high austenitizing temperatures, and after forging, many kinds of nonmetallic particles (VN, VC, TiN, etc.) precipitate during subsequent direct-cooling. These nonmetallic particles can therefore be used to produce an IAF microstructure instead of the more usual mixture of ferrite and pearlite after forging [24]. Precipitation takes place preferentially in austenite or ferrite grain boundaries, sub-boundaries, lattice defects such as dislocations, or at the interphase boundaries during the transformation. The particles precipitated inside austenite provide direct sources for IAF formation. Precipitates may deplete elements such as carbon, manganese, and silicon from the austenite. This depletion leads to a local increase in the driving force for the nucleation of ferrite from austenite at the inclusion surface [25]. Also, thermal strains that occur near the precipitate/austenite interface due to the difference in the thermal expansion coefficients of austenite and precipitate may also reduce the activation energy for the formation of a ferrite nucleus [26]. In addition, due to the high austenitizing temperature, coarse austenite grain structures are usually found in forging steels. When the austenite grain size is large, the number density of inclusions becomes large relative to boundary nucleation sites, favoring the development of IAF on these nonmetallic inclusions [21]. As a strong carbide forming element, W had been found to increase the amount and improve the stability of precipitates in steels [10-11]. As a result, the large amount of nonmetallic particles after W addition relative to that without W provide abundant sites for IAF nucleation, and higher content of IAF is therefore obtained (Figs. 1(b) and (c)).

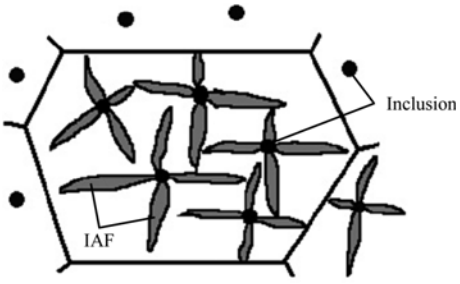

Fig. 2. Schematic diagram of IAF formation.

To study the effect of W on the formation of pearlite, the volume fractions of pearlite in C1, CW1, and CW5 steels were measured. After measurement, the mean values of the volume fraction of pearlite were obtained to be 31 %, 28 %, and 26 % in C1, CW1, and CW5 steels, respectively. This indicates that the growth of pearlite in both CW1 and CW5 steels is retarded after W addition, and the higher the content the W that is added, the more effectively pearlite growth is retarded.

3.1.2. Effect of W on the interlamellar spacing of pearlite

Since the interlamellar spacing of pearlite in ferritic-pearlitic steels is closely related to mechanical properties such as tensile strength and hardness [27-28], it is necessary to accurately measure the interlamellar spacing of pearlite. However, measurement is often complicated by the spacing variations within a given pearlite colony, those between different colonies, and those produced by the metallographic sectioning plane with respect to the orientation of the lamellae. Thus, the ability and the method used to measure the interlamellar spacing are vital in any attempt to correlate the spacing with the mechanical properties of ferritic-pearlitic steels. Fortunately, several efforts to measure interlamellar spacing have been made by many researchers [29-37]. Among these methods, that recommended by Underwood [32], which is used in the present work, is the simplest and most universal one to determine the mean true spacing by measuring the mean direct spacing. A schematic illustration of the measurement of interlamellar spacing of pearlite is shown in Fig. 3.

For a single pearlite colony, the mean direct spacing $\overline{S}_d$ is expressed as

$$\overline{S}_d = \frac{d_c}{n_c}, \tag{1}$$

where n_c is the number of cementite lamellae intercepted by the circle diameter d_c. In Fig. 3, $n_c = 10$. The mean true spacing $\overline{S}_t$ is given by

$$\overline{S}_t = \frac{\pi}{4} \cdot \overline{S}_d . \tag{2}$$

The measurement results of interlamellar spacing of pearl-

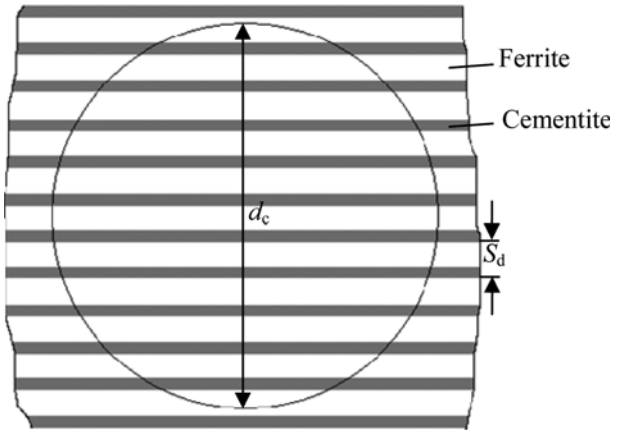

Fig. 3. Schematic illustration of the measurement of interlamellar spacing of pearlite.

Table 2. Interlamellar spacing of pearlite of C1, CW1, and CW5 steels

Specimens	S_d (nm)	S_t (nm)
C1	238	187
CW1	215	169
CW5	201	158

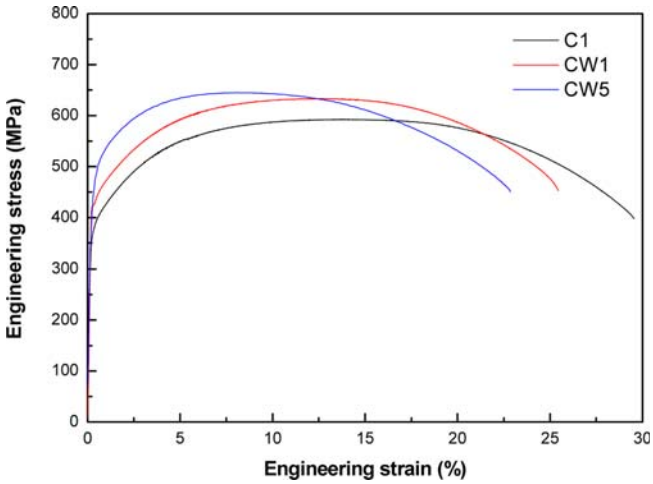

Fig. 4. Typical tensile curves of C1, CW1 and CW5 steels.

ite of C1, CW1, and CW5 steels are listed in Table 2. It is evident that the addition of W resulted in a significant decrease of interlamellar spacing of pearlite.

3.2. Mechanical properties

3.2.1. Tensile properties and hardness

The typical tensile curves of C1, CW1, and CW5 steels are shown in Fig. 4. The engineering stress-strain curves without apparent yield points can be simply divided into three stages, namely, elastic deformation, plastic deformation, and fracture. The tensile properties along with the hardness values of C1, CW1, and CW5 steels are presented in Table 3. The addition of W increased tensile strength and hardness, but it decreased elongation.

Figure 5 shows the tensile fracture morphologies of C1, CW1, and CW5 steels. All the fracture morphologies exhibit ductile characteristics with lots of dimples in the surfaces. However, the size and distribution of dimples changed after W addition. Smaller and more uniformly distributed dimples are observed in CW1 and CW5 steels compared with that in C1 steel.

3.2.2. Effect of W on mechanical properties

The strength of pearlite has been reported to follow a Hall-Petch type relationship with respect to the interlamellar spacing [27,28]. Several researchers have reported that the strength of ferritic-pearlitic steels is governed by pearlite, and the mechanical properties, including yield strength, ultimate tensile strength, elongation, and hardness, are considered to be greatly influenced by the interlamellar spacing of pearlite [36-38].

During the process of pearlite deformation, the ferrite in the pearlite is also deformed because ferrite is softer than cementite. Plastic deformation is always associated with the free movement of dislocations. During the plastic deformation process, large numbers of dislocations are generated in ferrite, especially in the plastically deformed zones. These dislocations interact with each other, restricting their own free movement. When the interlamellar spacing of pearlite is small, the movement of dislocations is more difficult in ferrite, which results in large numbers of dislocations existing in the matrix (Fig. 6), thus increasing the strength and hardness. This, in turn, causes a decrease of elongation. Therefore, the decrease of interlamellar spacing of pearlite after W addition is the direct cause of increased tensile strength and hardness.

As to the causes of increased strength after W addition, two others causes are considered. One is the solid solution strengthening induced by W addition, the other is the hardening induced by the fine precipitates in CW1 and CW5 steels. Abe *et al.* [39] has reported that W addition retards microstructural evolution at high temperature and improves the stability of precipitates in steel. The work of Park *et al.* [11] has shown that the addition of W in steels plays an

Table 3. Tensile properties and hardness of C1, CW1, and CW5 steels

Specimens	YS (MPa)	UTS (MPa)	Elongation (%)	Hardness (HV)
C1	363	593	29	185
CW1	374	624	26	217
CW5	383	645	23	223

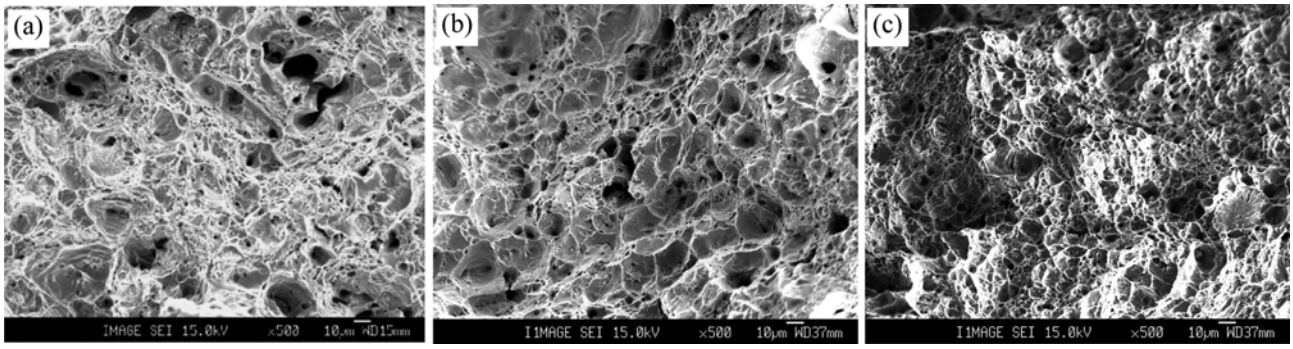

Fig. 5. Tensile fracture morphologies of (a) C1, (b) CW1, and (c) CW5 steels.

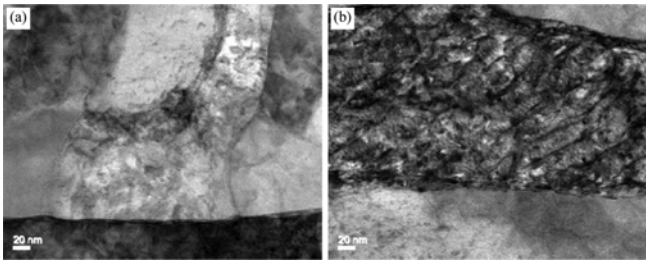

Fig. 6. TEM micrographs showing large numbers of dislocations exist in CW1 relative to C1. (a) C1; (b) CW1.

important role in retarding the growth of precipitates, and then fine precipitates can be obtained. With refinement of various precipitates, the barriers to dislocation motion increase with increasing interphase boundary. The increase of strength and hardness is caused, at least partly, by the refinement of precipitates after W addition in CW1 and CW5 steels.

Moreover, the formation of IAF, as reported by many researchers [40-42], also causes strength and hardness to increase to a certain extent.

3.3. Corrosion resistance

Figure 7 plots the potential against current density for the polarization of C1, CW1, and CW5 steels in both 1 % and 3.5 % NaCl solution. No passivation region appears in the curves, and the curve shape of C1 is similar to that of CW1 and CW5. However, the addition of W acts to render the potential and current density more positive and negative than that of C1, respectively. The corrosion resistance is enhanced

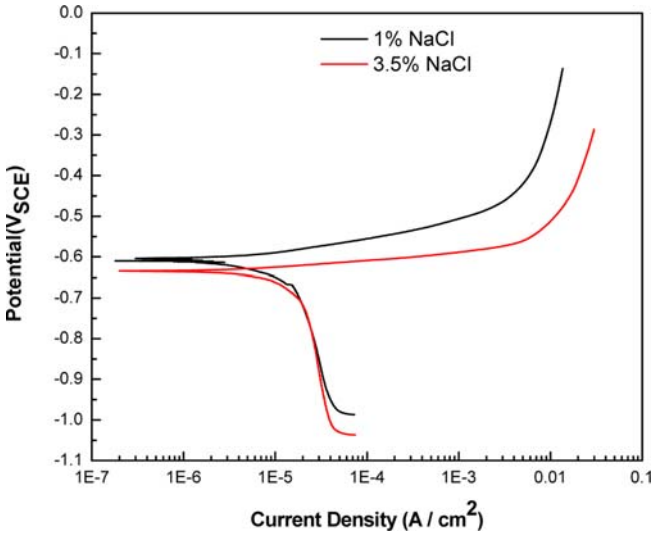

Fig. 8. Comparison of the polarization curves of C1 steel in NaCl solutions with different concentrations.

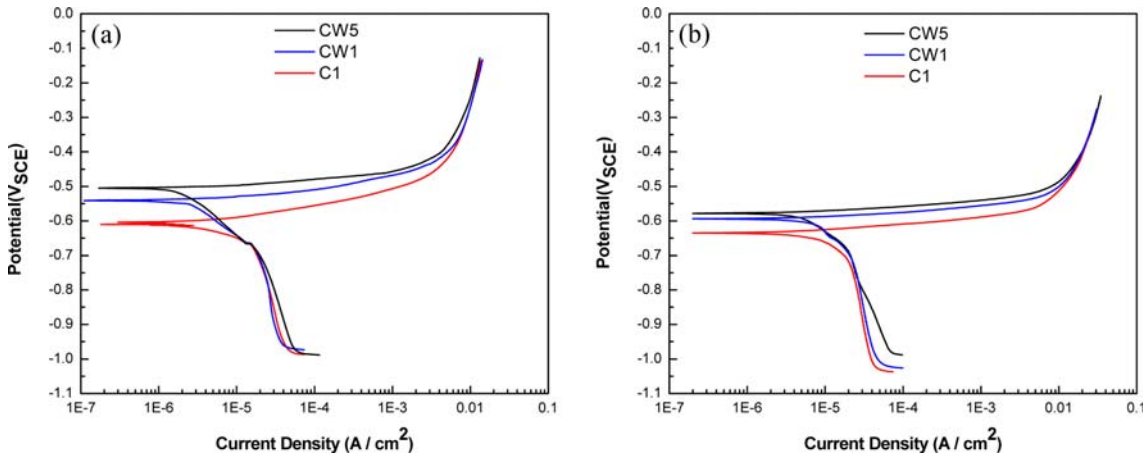

Fig. 7. Polarization curves of C1, CW1 and CW5 steels in (a) 1 % and (b) 3.5 % NaCl solutions.

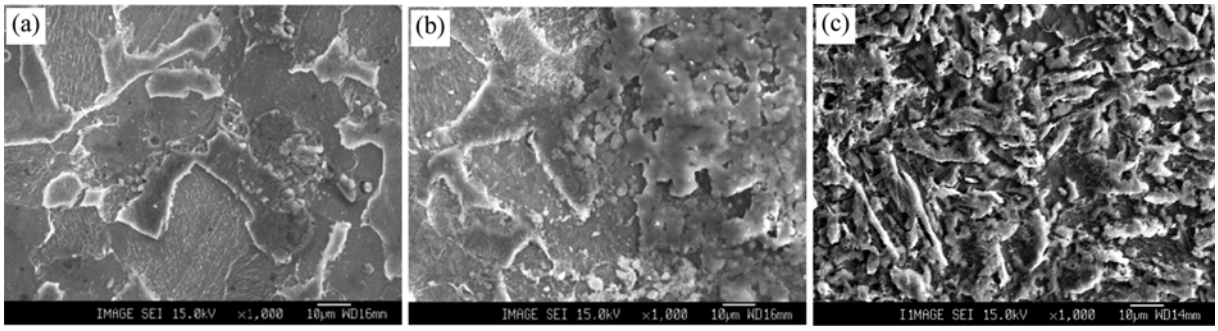

Fig. 9. SEM micrographs of the corroded surfaces in 3.5 % NaCl solution. (a) C1, (b) CW1, and (c) CW5.

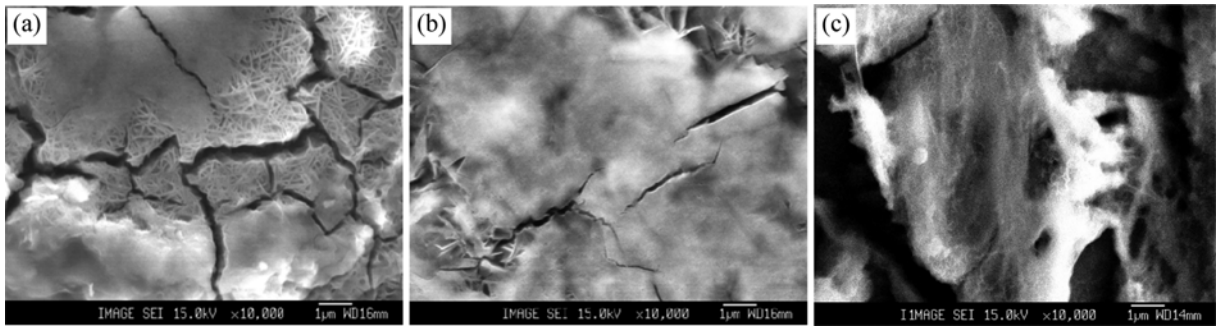

Fig. 10. SEM micrographs showing corrosion cracks in the corroded surfaces in 3.5 % NaCl solution: (a) C1, (b) CW1, and (c) CW5.

after W addition. Figure 8 shows the comparison of the polarization curves of C1 steel in NaCl solutions with various concentrations. It indicates that the change of concentration of NaCl has no obvious effect on polarization behavior; only the current density increases, and the corrosion potential moves negatively with increased concentration of NaCl. To evaluate the corrosion resistance comprehensively, another analysis of corrosion surfaces was carried out.

Figure 9 shows SEM micrographs of the corroded surfaces of C1, CW1, and CW5 steels in 3.5% NaCl solution. As shown in Figs. 9(a) and (b), CW1 steel shows a greater area of corrosion rust film than C1 steel. With further increase of the W content from 0.1% to 0.5%, almost the whole corroded surface is covered by a corrosion rust film, as shown in Fig. 9(c). Figure 10 shows typical SEM micrographs of the corrosion rust films. Large numbers of microcracks are distributed in the corrosion rust layers in C1 steel as seen in Fig. 10(a). However, a remarkable decrease in the quantity of microcracks is observed after W addition as shown in Figs. 10(b) and (c). The morphology of corrosion rust film reflects the corrosion resistance of steel. Generally, an intact corrosion rust film which contains few micocracks corresponds to high corrosion resistance of steel.

The beneficial effect of W addition on the corrosion resistance of steels has been reported by many researchers [14, 43-46]. It has been suggested that the enhancement of corrosion resistance is directly connected with the formation of a protective film. An earlier work about stainless steel showed that alloyed W is present in the passive layer under the 6^+ oxidation state [43]. The mechanism was the direct interaction of W with H_2O to form insoluble WO_3 in the passive film, followed by the interaction of WO_3 with other oxides to form a complex oxide film. For low-alloy steel, W addition has also been found to be effective to retard corrosion due to the formation of a protective film [45]. In brief, W promotes the formation of a protective film on the surface of steel, which is considered to be the direct cause of enhanced corrosion resistance after W addition.

4. CONCLUSIONS

In the present investigation, the effect of W addition on the microstructure, tensile properties, Vickers hardness, and corrosion resistance of S355NL forging steel was studied. The major conclusions derived from this work are the following.

(1) The addition of W favors the formation of IAF in microalloyed forging steel. W has a significant effect on the decreased interlamellar spacing of pearlite.

(2) W plays a role in increasing the tensile strength and hardness of S355NL forging steel. The decreased interlamellar spacing of pearlite is considered to be the direct cause of the enhanced tensile strength and hardness.

(3) After W addition, the corrosion rust film is intact. There are far fewer microcracks in the corrosion rust films of the specimens with W than there are in that without W. In

conclusion, W alloying has been found to be beneficial to the enhancement of corrosion resistance.

ACKNOWLEDGMENTS

This work was financially supported by the Ministry of Knowledge and Economy, Korea under the program (2009-D-2-A-Y0-B-07) of Leading Industry Development for Dongnam Economic Region. The authors wish to thank Dae Won Yun for his help in conducting the corrosion tests.

REFERENCES

1. P. Farsetti and A. Blarasin, *Int. J. Fatigue* **10**, 153 (1988).
2. R. Kuziak, T. Bold, and Y. W. Cheng, *J. Mater. Process. Technol*. **53**, 255 (1995).
3. G. Krauss, *Steels: Processing, Structure, and Performance*, p. 230, ASM International, Ohio (2005).
4. H. K. Sung, S. Y. Shin, B. Hwang, C. G. Lee, N. J. Kim, and S. Lee, *Korean J. Met. Mater.* **48**, 798 (2010).
5. A. Elmalki Alaoui, D. Thevenet, and A. Zeghloul, *Fatigue Fract. Eng. Mater. Struct*. **30**, 489 (2007).
6. N. Lautrou, D. Thevenet, and J.-Y. Cognard, *Fatigue Fract. Eng. Mater. Struct*. **32**, 403 (2009).
7. P. Y. Decreuse, S. Pommier, L. Gentot, and S. Pattofatto, *Int. J. Fatigue* **31**, 1733 (2009).
8. A. El Malki Alaoui, D. Thevenet, and A. Zeghloul, *Eng. Fract. Mech*. **76**, 2359 (2009).
9. B. H. Li, Y. Liu, J. Li, S. J. Gao, H. Cao, and L. He, *Mater. Des*. **31**, 877 (2010).
10. Y. Zhang, Y. F. Sun, S. K. Guan, X. Deng, and X. Y. Yan, *Mater. Sci. Eng. A* **478**, 214 (2008).
11. J. S. Park, S. J. Kim, and C. S. Lee, *Mater. Sci. Eng. A* **298**, 127 (2001).
12. N. H. Heo and H. C. Lee, *Scr. Metall. Mater.* **33**, 2031 (1995).
13. W. S. Ji, Y.-W. Jang, and J.-G. Kim, *Met. Mater. Int*. **17**, 463 (2011).
14. S. H. Mousavi Anijdan, A. Bahrami, N. Varahram, and P. Davamic, *Mater. Sci. Eng. A* **454-455**, 623 (2007).
15. M. K. Ahn, H. S. Kwon, and H. M. Lee, *Corros. Sci*. **40**, 307 (1998).
16. A. Belfrouh, C. Masson, D. Vouagner, A. M. De Becdelievre, N. S. Parkash, and J. P. Audouard, *Corros. Sci*. **38**, 1639 (1996).
17. I. Madariaga and I. Gutiérrez, *Scr. Mater.* **37**, 1185 (1997).
18. C. García de Andrés, C. Capdevila, I. Madariaga, and I. Gutiérrez, *Scr. Mater.* **45**, 709 (2001).
19. J.-H. Shim, Y. M. Cho, S. H. Chung, J.-D. Shim, and D. N. Lee, *Acta Metall*. **47**, 2751 (1999).
20. T. Pan, Z.-G. Yang, C. Zhang, B.-Z. Bai, and H.-S. Fang, *Mater. Sci. Eng. A* **438-440**, 1128 (2006).
21. H. K. D. H. Bhadeshia, *Bainite in Steels, 2nd ed*., p. 238, The University Press, Cambridge, London (2001).
22. R. A. Ricks, P. R. Howell, and G. S. Barritte, *J. Mater. Sci*. **17**, 732 (1982).
23. J. R. Yang and H. K. D. H. Bhadeshia, *Advances in Welding Science and Technology* (ed. S.A. David), p. 187, ASM, Metals Park, Ohio (1986).
24. M. A. Linaza, J. L. Romero, J. M. Rodríguez-Ibabe, and J. J. Urcola, *Scr. Metall. Mater.* **29**, 1217 (1993).
25. J. M. Gregg and H. K. D. H. Bhadeshia, *Acta Metall. Mater*. **42**, 3321 (1994).
26. T. Pan, Z. G Yang, B. Z. Bai, and H. S. Fang, *Acta Metall. Sin*. **39**, 1037 (2003).
27. A. R. Marder and B. L. Bramfitt, *Metall. Trans. A* **7**, 365 (1976).
28. K. K. Ray and D. Mondal, *Acta Metall. Mater.* **39**, 2201 (1991).
29. G. E. Pellissier, M. F. Hawekes, W. A. Johnson, and R. F. Mehl, *Trans. ASM* **30**, 1049 (1942).
30. J. W. Cahn and R. L. Fullman, *Trans. AIME* **206**, 610 (1956).
31. G. Birkbeck and T. C. Wells, *Trans. AIME* **242**, 2217 (1968).
32. E. E. Underwood, *Quantitative Stereology*, p. 73, Addison-Wesley, Reading, Massachusetts (1970).
33. A. Roósz, Z. Gácsi, and M. K. Baan, *Metallography* **13**, 299 (1980).
34. G. F. Vander Voort, *Metallography* **17**, 1 (1984).
35. J. F. Tilbury, T. D. Motishaw, and G. D. W. Smith, *Metallography* **19**, 243 (1986).
36. H. S. Fong, *Metallography* **23**, 173 (1989).
37. F. G. Caballero, C. García de Andrés, and C. Capdevila, *Mater. Charact*. **45**, 111 (2000).
38. O. P. Modi, N. Deshmukh, D. P. Mondal, A. K. Jha, A. H. Yegneswaran, and H. K. Khaira, *Mater. Charact*. **46**, 347 (2001).
39. F. Abe, T. Noda, H. Araki, and S. Nakazawa, *J. Nucl. Mater.* **179-181**, 663 (1991).
40. M. Díaz, I. Madariaga, J. M. Rodriguez-Ibabe, and I. Gutierrez, *J. Constr. Steel Res*. **46**, 413 (1998).
41. M. C. Zhao, K. Yang, and Y. Y. Shan, *Mater. Lett*. **57**, 1496 (2003).
42. F. R. Xiao, B. Liao, Y. Y. Shan, G. Y. Qiao, Y. Zhong, C. L. Zhang, and K. Yang, *Mater. Sci. Eng. A* **431**, 41 (2006).
43. A. Irhzo, Y. Segui, N. Bui, and F. Dabosi, *Corros. Sci*. **26**, 769 (1986).
44. J. Chen and J. K. Wu, *Corros. Sci*. **30**, 53 (1990).
45. M. Itagaki, R. Nozue, K. Watanabe, H. Katayama, and K. Noda, *Corros. Sci*. **46**, 1301 (2004).
46. D. W. Kim and H. Kim, *Korean J. Met. Mater.* **48**, 523 (2010).